

Single Particle Spectroscopy Study of Metal-Film-Induced Tuning of Silver Nanoparticle Plasmon Resonances[†]

Min Hu,^{*,§} Amitabh Ghoshal,[‡] Manuel Marquez,^{||} and Pieter G. Kik^{*,‡}

CREOL, The College of Optics and Photonics, University of Central Florida, Orlando, Florida 32816, Information and Quantum Systems Laboratory, Hewlett-Packard Laboratories, 1501 Page Mill Road, Palo Alto, California 94304, and YNano LLC, 14148 Riverdowns South Drive, Midlothian, Virginia 23113

Received: December 1, 2009; Revised Manuscript Received: February 15, 2010

We present an experimental study of the tunability of the silver nanoparticle localized plasmon resonance in close proximity to a gold film. Broad-band tuning of the silver particle plasmon resonance from blue wavelengths into the near-IR region can be achieved due to strong electromagnetic coupling between the nanoparticle and the metal film. When the thickness of a thin silica spacer layer between the metal nanoparticle and the metal film is altered, the resonance frequency shifts. Single particle spectroscopy of over 250 isolated silver nanoparticles revealed evidence for the excitation of both horizontal and vertical plasmon modes. Distinct resonance features observed in the scattering spectra were assigned to specific modes based on a dipole–dipole interaction model. The experimental results suggest that low-loss silver nanoparticles can be used in surface-enhanced spectroscopy studies throughout the entire visible spectrum. The use of frequency-tuned spherical metal nanoparticles on solid substrates could lead to thermally stable substrates for plasmon-enhanced sensing applications, including surface-enhanced Raman scattering and refractive index based biodetection methods.

1. Introduction

Photonic devices based on metal nanostructures have drawn intensive research interest. The research is driven in large part by the unique optical resonances that can occur on such nanostructures, known as surface plasmon resonances. Surface plasmon resonances involve the collective oscillation of free electrons in the metal, resulting in strongly confined and enhanced electric fields, often at visible frequencies. This has led to many surprising and technologically relevant optical phenomena, including plasmon-enhanced nonlinear absorption and refraction,^{1,2} plasmon-enhanced fluorescence,^{3,4} and surface-enhanced Raman spectroscopy (SERS).^{5,6} In these and related fields, control over the plasmon resonance frequency is essential. The localized surface plasmon resonances (LSPR) of small metal nanoparticles are extremely sensitive to the particle shape, size, composition, and dielectric constant of the surrounding dielectric materials.⁷ By modification of these parameters, the LSPR can be tuned throughout the visible and near-infrared spectral region. An alternative approach to realize tuning of metal nanoparticle plasmon resonances is to introduce a thin conducting film, for example a thin metal film, in the vicinity of metal nanoparticles. The large negative dielectric function of conductors dramatically alters the dielectric environment of the particles, resulting in a significant modification of the plasmon resonance frequency. The interaction between metal nanoparticles and metal films exhibits several features that make it attractive for nanophotonic applications. First, such a particle–film system effectively acts as an optical antenna structure and can localize visible radiation to subwavelength dimensions and thus control light–matter interactions at the nanoscale. Control over the particle–substrate interaction can be used to achieve this confinement at specific

wavelengths, for example, matched to a molecular transition. Second, large electric field enhancements occur at the particle–film gap, and consequently any of the field-enhanced effects discussed before are also expected to occur in a coupled particle–surface system. Other examples of applications that will benefit from the understanding and control of the LSPR include nanoparticle biomarkers, plasmon-based ultrasensitive chemo- and biosensors, and ultrafast optical switches based on plasmon-enhanced nonlinearity.

The theoretical study of plasmon coupling between metal nanoparticles and metal films dates back to the 1980s^{8–10} and still draws intense research interest both theoretically^{11–14} and experimentally^{15–24} due to its numerous applications. For example, Holland and Hall observed a frequency shift of a silver island film near a silver thin film in their experimental investigations. Later, Tadashi et al. verified the frequency shift and multiple resonances based on numerical simulations. Recently, Martin and co-workers have studied the optical properties of rectangular particles above a metallic slab based on a numerical calculation where a dielectric spacer of a few tens of nanometers was added between the particle and the slab. They found in their calculation that the resonance wavelength of the particle depends on both the spacer thickness and its susceptibility.^{25,26} Nordlander and co-workers studied the plasmon coupling between a metal nanoshell and a metal substrate and employed a plasmon hybridization method to explain their experimental results on nanoparticle resonance tuning.¹² However, most of the experimental research involved measurements on regular and irregular ensembles of nanoparticles near metal films, and few results have been reported for the response of a single nanoparticle when placed close to a metal film, possibly due to the relatively weak scattering from single nanoparticles. Only recently single particle studies were carried out on gold particles near a gold substrate²³ and for solid gold nanoparticles and gold nanoshells near dielectric surfaces.²⁷ It is extremely important to perform single particle experiments for at least two

[†] Part of the “Martin Moskovits Festschrift”.

^{*} Author to whom correspondence should be addressed, kik@creol.ucf.edu.

[‡] University of Central Florida.

[§] Hewlett-Packard Laboratories.

^{||} YNano LLC.

reasons. First, the single particle spectroscopy removes any inhomogeneous contributions from the measurement, which can obscure subtle features in the optical spectra and prevent the accurate determination of resonance line widths. Second, since most of the theoretical work considered a single particle above a film, experimental studies on single particles near conducting surfaces immediately allow direct comparison between the experiment and the theory. Recent progress and interest in optical microscopy has enabled the study of single metal nanoparticles.^{28–31} The pioneering work was done by Feldmann and co-workers,^{32,33} who systematically studied the optical properties of noble metal nanoparticles at the single particle level. Due to the reduction in the inhomogeneous broadening effects from different sizes and shapes present in the sample,³⁴ measurements on single particles can provide a more detailed understanding of the optical response of nanoparticles. This is also important for plasmon-based single particle molecular sensing applications where a small line width is preferred, as the sensitivity is strongly dependent on the quality factor of $Q = f_{\text{res}}/\Gamma_{\text{hom}}$, where Γ_{hom} is the homogeneous line width and f_{res} is the resonance frequency.

In this work, we present a single particle spectroscopy study of silver nanospheres above a gold substrate. This system could be preferable over the previously mentioned system of gold particles near a gold film due to the relatively low damping of electrons in silver, potentially allowing for sharp optical resonances, a high Q factor, and large field enhancements. The particle–film distance was controlled by an intermediate spacer layer with different thickness. The plasmon resonance of the spherical silver nanoparticles was found to be tunable throughout the entire visible spectrum. The presence of both horizontally and vertically polarized plasmon resonances is demonstrated in our experiments, and the spectral results can be understood using a dipole–dipole interaction model. The amount of red shift of the nanoparticle resonances appears to depend strongly on the polarization of the excited mode.

2. Experimental Section

Silver nanoparticle colloid solution (average particle diameter 60 nm) was obtained from Ted Pella (British Biocell International). The aqueous nanoparticle solution contains a trace amount of sodium citrate ($\text{Na}_3\text{C}_6\text{H}_5\text{O}_7$). The extinction spectrum of the undiluted solution was measured using a Cary500 UV–vis–NIR spectrophotometer and showed a clear extinction peak at 430 nm with a full width at half-maximum (fwhm) of 115 nm due to the dipolar plasmon resonance on the silver nanoparticles. Glass slides (Erie Scientific) were sonicated for 20 min in deionized water and ethylene alcohol and subsequently dried in a nitrogen stream. Continuous gold films with a thickness of 50 nm were deposited on four glass slides with a Precision Etching Coating System (PECS, model 682 PECS, Gatan, Inc.) using an ion beam energy of 10 keV. The thickness was controlled using a quartz-crystal film-thickness monitor. Subsequently, thin silica (SiO_2) spacer layers with thicknesses of 10, 20, and 40 nm were deposited directly on the gold-coated glass slides at a rate of 0.9 nm/s using a UnAxis PlasmaTherm 790 PECVD/RIE Reactor, at a temperature of 250 °C. A 0.5 wt % poly(vinylpyrrolidone) (PVP) solution was prepared by adding 50 mg of PVP (molecular weight ~ 55000) to 10 mL of water. The polymer solution was sonicated for 5 min, and heated slightly until a clear solution was obtained. To prepare the samples, the original nanoparticle solutions were first diluted twice in deionized water. Then 1 mL of the diluted nanoparticle solution was mixed homogeneously with 1 mL of the PVP

solution in order to improve the immobilization of nanoparticles on substrate surfaces as well as to prevent nanoparticle agglomeration on the substrate. A micropipet (0.5 μL) was used to deliver a small drop of the diluted nanoparticle/PVP solution on the prepared substrates. After 10 s the liquid drop was removed from the substrate by a nitrogen stream. This procedure was repeated if necessary until a final particle density of ~ 10 nanoparticles per $30 \times 30 \mu\text{m}^2$ was reached as observed in dark field microscopy. Some residual PVP may remain on the sample after this procedure. The nanoparticle deposition was immediately followed by a single particle spectroscopy characterization to minimize the probability of nanoparticle degradation.

Optical Studies—Single Nanoparticle Spectroscopy. An Olympus BX-51 reflected light optical microscope equipped with standard dark-field optics was used for single particle dark field (DF) microscopy and spectroscopy. The illumination source consists of a standard 100 W halogen lamp (Olympus U-LH 100 L-3). The factory heat filter (a ~ 700 nm short-pass filter) was removed from the lamp housing to provide sufficient near-IR illumination. The Rayleigh scattering from individual metal nanoparticles was collected using a 50 \times dark-field objective (Olympus UMPLFL 50 \times BD). Diffraction-limited microscopy images were obtained using a standard digital camera. For single particle spectroscopy the scattered light was focused onto a multimode optical fiber (Ocean Optics) and directed to the entrance slit of a monochromator (Acton Research SpectraPro-2300i). At this magnification the estimated sampling area is $\sim 13 \mu\text{m}^2$, allowing for selective collection of scattered light from individual nanoparticles deposited on the substrate at the previously specified low particle density. The collected light was dispersed using a grating (150 grooves/mm, blaze wavelength 500 nm). Spectra were recorded using a thermoelectrically cooled CCD camera (Andor, DU401-BRDD). Normalized Rayleigh scattering spectra I_{sc} from individual particles were obtained as a function of wavelength λ using the relation $I_{\text{sc}}(\lambda) = (S - R)/R$. Here S is the collected signal from an area containing a nanoparticle and R represents the signal collected from a nearby area of the sample (identical sampling area but without particles). Acquisition times for the spectra were 10 to 20 s. All experiments were conducted in an ambient lab environment.

3. Results and Discussion

Figure 1a shows a schematic of the DF illumination setup used in the experiments. High angle illumination leads to an induced oscillating dipole on the nanoparticle. The Rayleigh scattered light from the metal nanoparticle is collected by the same objective that enables the DF illumination. An example image of a single particle as recorded on the camera is included in the sketch. For reference Figure 1b shows a normalized extinction spectrum of the silver nanoparticles used in our experiments in aqueous solution (black solid line). The strong single extinction peak at 430 nm demonstrates that the solution predominantly contains isolated nearly spherical nanoparticles, as opposed to particle agglomerates, or silver nanoprisms, nanorods, etc., as these exhibit broader and/or red-shifted resonances. It is well-known from Mie theory that spherical metal nanoparticles in a homogeneous medium exhibit a dipolar resonance with a resonance frequency that is largely determined by the dielectric function of the particle and that of the surrounding medium. On the basis of literature values for the dielectric function of silver, the dipolar plasmon resonance of silver nanoparticles in aqueous solution occurs at ~ 380 nm (350 nm in air) according to Mie theory, compared to the resonance

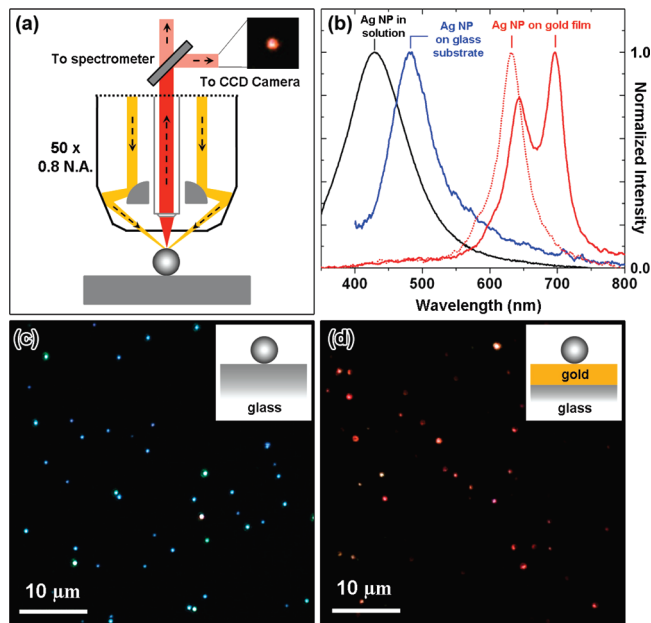


Figure 1. (a) Schematic of the experimental arrangement for single particle dark field microscopy and spectroscopy using a reflected light dark field objective. (b) UV-vis extinction spectrum of an aqueous solution of spherical silver nanoparticles with an average diameter of 60 ± 5 nm used in the experiment (black line); Examples of optical scattering spectra for single silver nanoparticles deposited on a glass substrate (blue line) and on a 50 nm gold film (red solid line and dotted line). (c) and (d) True color dark field microscopy images of isolated silver nanoparticles on a plain glass substrate (c) and on a 50 nm gold film deposited on a glass substrate (d). The insets in (c) and (d) schematically show the cross section of the corresponding substrates.

at 430 nm observed here. Part of this red shift is attributed to retardation effects which are known to reduce the resonance frequency for particles with a size that is significant relative to the incident wavelength or the field penetration depth. To verify this, numerical simulations were carried out (not shown) to determine the resonance wavelength of 60 nm diameter silver nanoparticles in water ($n \approx 1.33$) based on the literature dielectric function of silver, resulting in a resonance wavelength of ~ 415 nm. The remaining 15 nm red shift observed in our experiments may be related to the presence of a thin silver oxide coating on the silver nanoparticles or to the presence of a small amount of citrate around the nanoparticles in solution. Figure 1c shows a real-color DF microscopy image of single silver nanoparticles deposited on an uncoated glass (SiO_2) substrate. Most of the nanoparticles were found to have a blue or blue-green appearance. The similarity in color of the single nanoparticles suggests that the size and the shape of the nanoparticles are relatively uniform or that any spectral variations occur outside the sensitivity range of the camera used. A small fraction ($\sim 1\%$) of the particles on the sample appeared red, possibly due to the formation of few-particle aggregates or the existence of a small fraction of large or nonspherical particles in the solution. Figure 1d shows a DF image of isolated silver nanoparticles from the same nanoparticle solution used to prepare the sample shown in Figure 1c but deposited on a 50 nm gold film deposited on a glass substrate. The silver nanoparticles deposited on the gold film clearly appear red or orange-red, in sharp contrast to the blue appearance of similar particles observed in Figure 1c. To quantify the red shift induced by the gold film, Figure 1b includes typical scattering spectra observed from individual particles on different substrates. Most

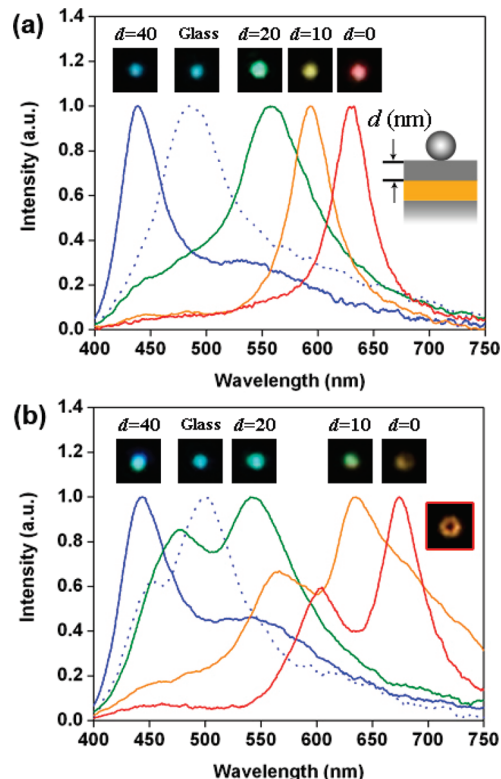


Figure 2. Examples of optical scattering spectra for silver nanoparticles on different substrates exhibiting a single resonance peak (a) and exhibiting two resonance peaks (b). The inset in (a) schematically shows the cross section of the substrate with a silica spacer layer of varying thickness d (nm) on top of a 50 nm gold film supported by a glass substrate. Note that the cross sections of the substrates are the same for (a) and (b), but the spectra were taken from different individual nanoparticles. Above each spectrum in (a) and (b) is the corresponding true color dark field image of the silver nanoparticle. The dotted lines represent single particle spectra of silver nanoparticles on plain glass substrate. The highlighted rightmost dark field image in (b) is an example of a vertically polarized resonance of a silver particle directly on a gold film, leading to a donut-shaped optical image.

of the particles on the glass substrate exhibit a peak resonance wavelength in the range 450–490 nm. Figure 1b shows a typical spectrum from a Ag nanoparticle on the glass substrate, with a peak scattering wavelength of 490 nm. This wavelength lies close to the single particle resonance wavelength observed in solution phase (430 nm). The difference in resonance for substrate and solution phase is discussed in more detail below. A representative spectrum of a silver particle on the Au-coated sample is included in Figure 1b (thin red line). A sharp scattering spectrum is observed peaking at 640 nm, 150 nm red shifted compared the peak-wavelength observed for Ag nanoparticles on the glass substrate. Interestingly, some particles show two clearly separated scattering peaks, while other particles show one predominant peak with a weaker shoulder. Note that in Figure 1b all the spectra have been normalized in order to facilitate direct comparison of peak positions. However, it should be noted that the particle on the Au-coated samples shows stronger scattering intensities compared to those observed on glass, by a factor of 2–3.

To investigate the plasmon resonance shift in the presence of a metallic substrate in more detail, we fabricated different substrates with silica spacer layers of varying thickness d . The cross section of such a substrate is sketched in Figure 2a. Representative Rayleigh scattering spectra of isolated silver nanoparticles on these substrates as well as the DF microscopy

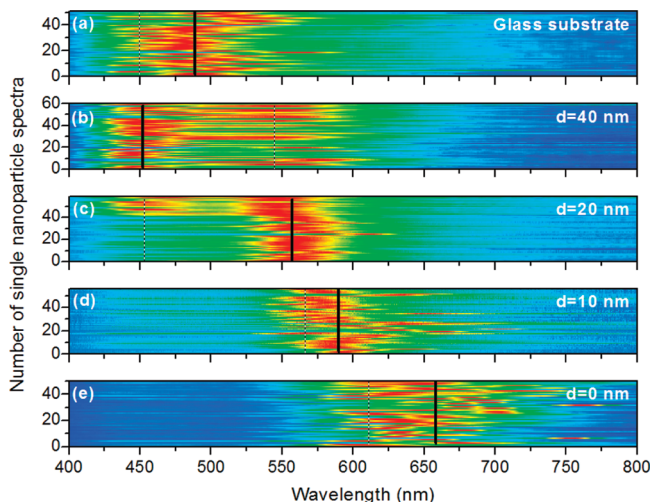


Figure 3. Normalized single particle spectra of individual silver nanoparticles on different substrates, shown as a function of measurement number. The different panels represent different substrates: (a) plain glass substrate, (b–d) substrates with a silica spacer layer of varied thickness d (nm) on top of a gold thin film of 50 nm supported by a glass substrate with $d = 40, 20,$ and 10 nm, respectively, (e) substrate with no spacer layer ($d = 0$ nm) on top of the 50 nm thick gold thin film supported by a glass substrate. The red color indicates the largest observed intensity and corresponds to the location of the plasmon resonance of the silver nanoparticles. The vertical black thick lines and the black dotted lines in each panel show the primary and the secondary plasmon resonances, respectively.

images of the corresponding nanoparticle are also displayed. The spectra were normalized to their peak intensity and are shown at a spectral resolution of 10 nm. Generally the spectra can be divided into two groups for each substrate configuration, namely, single-peak spectra and double-peak spectra, as shown in parts a and b of Figure 2, respectively. The spectra obtained from Ag particles on the glass substrate have been included as a reference. Several points should be noted. First, by varying the thickness of the spacer layer between the gold film and the nanoparticles, the observed plasmon resonance of the silver nanoparticle can be tuned across the entire visible spectrum, with peak wavelengths observed from 440 to 670 nm. Note that this includes Ag particles with a resonance close to 632 nm, coinciding with a common HeNe laser wavelength. Consequently, this type of tuning scheme could make Ag nanoparticles a viable structure in single particle SERS studies using a relatively low-cost narrow line laser source. We could not verify the presence of any additional scattering peaks in the IR region due to the detection limit of the detector. Second, for those particles which exhibit a double-peak scattering spectrum, both peaks appear near the peak wavelength observed for single-peak spectra. In the case of the $d = 40$ nm substrate this is seen to lead to resonances that lie to the high-energy side of the single particle spectra obtained from the glass substrate. When the thickness d is much greater than 100 nm (data not shown), the resonance wavelength matches that observed on the glass reference. Third, for a sufficiently small thickness ($d < 20$ nm), some nanoparticles are seen to generate a donut-shaped optical pattern in the DF image as shown in the inset on the far right in Figure 2b. This type of pattern is known to be indicative of a vertically polarized scatterer.

To verify the reproducibility of the observed frequency tuning, we have measured over 250 single nanoparticle spectra (50–60 spectra for each substrate). The results are summarized in Figure 3. Each panel of Figure 3 contains 50–60 scattering spectra, each individually normalized to 1. The color scale represents

the measured scattering intensity of a single nanoparticle, with red indicating higher scattering intensity. The y-axis indicates the number of the spectrum in the order it was taken. The averaged primary and secondary plasmon resonance wavelengths have been highlighted with a solid and dotted lines as guide to eyes in each panel respectively. It is clear that decreasing the spacer thickness leads to a general red shift in the plasmon resonance despite a significant variation in central frequency at each spacer layer thickness. The variations observed in the central frequency may be related to variations in film thickness and to surface roughness, leading to variations in local particle environment. The maximum observed resonance shift corresponds to a resonance peak at a wavelength of 760 nm in the near-IR region (panel e). The spectra of nanoparticles on a plain glass slide are shown in Figure 3a. Interestingly, the resonance frequency of the silver particles on the glass slide exhibits an average resonance frequency that lies lower than many of the observed scattering peaks observed on the sample with a spacer thickness of 40 nm. Possible origins of this observation are discussed below.

The large red shift of plasmon resonance observed in our experiment agrees qualitatively with the predictions made in the aforementioned theoretical studies. To first order the red shift of the particle resonance frequency can be understood using the image dipole model as shown in Figure 4. Under our dark field illumination conditions, the incident light wave can be decomposed into s-polarized and p-polarized waves. The former excites lateral (along the substrate surface) electron oscillation in the metal nanoparticle while the latter excites both lateral and normal oscillation (i.e., along the substrate surface normal). In the following discussion we consider the p-polarized wave since it contains both the horizontal and normal field components. In this case the vertical component of the incident electric field ($E_{in,z}$) is dominant over the horizontal component ($E_{in,x}$) since the light is incident light at an angle of $\sim 75^\circ$ relative to the surface normal for the DF microscope objective used. The incident light excites lateral and normal charge motion in the metal particle. At low frequencies (well below the plasma frequency of the metal film), any charge distribution in the metal particle induces a surface charge distribution on the film, with a field distribution above the metal surface corresponding to the apparent presence of the sketched image charge distribution in the metal film. When the distance from the particle to the metal film is small, a lateral particle polarization oscillating at low frequency leads to an antiparallel image dipole in the substrate, as shown in the central panel in Figure 4. This antiparallel charge arrangement can be seen to reduce the internal field in the particle, resulting in a reduced resonance frequency. Similarly, a normal particle polarization can be seen to lead to the development of an image dipole that is aligned parallel to the particle dipole, resulting again in a reduction of plasmon resonance frequency. In addition, the dipole–dipole interaction decreases with increasing distance of the particle from the metal surface, suggesting that the red shift will be dependent on particle–metal surface separation, as observed experimentally.

While the simple image dipole interaction model described above explains the observation of an increasing red shift for decreasing spacer thickness, several additional factors play a role. First, from electrostatic considerations it can be shown that the lateral arrangement in the central panel leads to a smaller change in the resonance frequency than the normal arrangement shown in the right panel. This means that under excitation with lateral and normal field components, two different amounts of

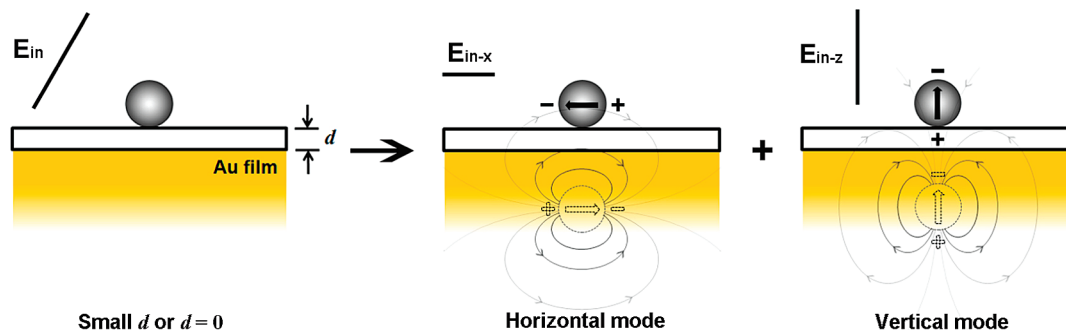


Figure 4. Schematic representation of dipole–dipole interaction for the particle–Au–film system with silica spacer layers of small thickness d . The electric field (E_{in}) of the p-polarized incident wave is also shown. Both the horizontal and vertical localized surface plasmon modes can be excited on the particle.

red shift are expected for a given particle–surface separation. Second, the antiparallel dipole orientation in the central panel is quadrupolar in nature, whereas the parallel dipole orientation in the right panel is dipolar in nature. For small particles and small particle–surface separations, a quadrupolar charge distribution leads to a low scattering efficiency, whereas a dipolar charge distribution leads to efficient radiation. Third, the normal image dipole can interact with the particle only through near-field interactions (i.e., at small particle–surface distances), whereas the lateral dipole can interact with the metal surface via the near-field as well as through radiative processes (reflection of scattered light).

With the considerations given above, we can now understand several experimental observations. We first consider the experimental results of thin spacer layers with a thickness d of 20, 10, and 0 nm. For these thicknesses, several particles exhibited two resonance peaks; see Figure 2b. These are tentatively attributed to the horizontal mode and vertical mode based on the image dipole model. In the case of the vertical mode, an electrostatic analysis shows that the image dipole generates an electric field that is two times stronger at the place of the original dipole than in the case of the horizontal mode; i.e., the vertical mode should have a significantly more red shifted resonance compared to the horizontal mode. Thus, the longer wavelength peaks for those substrates with smaller spacer layer thickness ($d = 20, 10, \text{ and } 0 \text{ nm}$ in Figure 2b) are assigned to the vertical mode while the shorter wavelength peaks are attributed to horizontal modes.

For very large values of thickness d , the particle resonance frequency is expected to converge to the value observed on the glass substrate. This was confirmed experimentally (not shown) using a $d > 1 \mu\text{m}$ thick deposited oxide layer. In this case, the polarizability of the glass or SiO_2 film ($n \approx 1.45$) still contributes a small red shift relative to the value in aqueous solution ($n \approx 1.33$), which can be interpreted as being due to a partial image charge formed in the substrate. This red shift is also expected to be polarization-dependent, analogous to the idealized case of a complete lateral or normal image dipole. Occasionally a very weak shoulder is observed at $\sim 450 \text{ nm}$ (see Figure 2b and 3a), which may be related to a small contribution of lateral polarization, while the 490 nm peak may be related to the normal mode. For an intermediate silica spacer layer thickness d comparable to the size of the nanoparticle (particle diameter $\sim 60 \text{ nm}$), the system becomes more complicated, since the polarizability of the silica film as well as the charge response in the metal film both affect the particle resonance frequency.

While the previous discussion can account for several of the observed features, two additional possibly significant factors

were not considered. First, the interacting dipole model assumes an ideal metal substrate (frequencies well below the plasma frequency) that can form a complete image dipole. However the frequencies observed here lie close to the surface plasmon resonance frequency ω_{SP} of a gold– SiO_2 interface, necessitating the consideration of the frequency-dependent metal dielectric function. At these high frequencies incomplete image dipoles are expected to form, and additionally interactions could occur between particle modes and surface plasmon modes excited on the film. While the present study cannot unambiguously determine the origin of the increased resonance frequency for $d = 40 \text{ nm}$, it is possible that such interactions play a role. Second, the dipole interaction model does not take into account the finite size of the nanoparticle and the inhomogeneous nature of the image dipole field and therefore does not consider the likely excitation of multipolar modes on the particle and their radiation efficiency. Further experiments are needed to investigate particle–film interactions in this interaction regime.

4. Summary and Conclusions

In summary, we have demonstrated a large localized surface plasmon resonance tunability for isolated silver nanospheres near a metal thin film by changing the distance between the particle and the metal film. Single-particle spectroscopy measurements revealed that the localized plasmon resonance for silver nanoparticles can be tuned from the near-UV into the near-IR by varying the coupling strength of the particle and the film. Plasmon resonance splitting was observed in single particle scattering spectra, which was attributed to the excitation of both horizontal and vertical plasmon modes. A dipole–dipole interaction model was used to qualitatively explain the observed red shift of the particle resonance and to assign the different resonant modes in our experiments. The high tunability of particle plasmon resonance in combination with resonantly enhanced electric fields in the particle–film gap could prove useful for surface-enhanced optical spectroscopy as well as chemo- and biosensing.

Acknowledgment. This work was supported in part by the National Science Foundation (CAREER Award ECCS-0644228) and by the University of South Florida Center for Biological Defense.

References and Notes

- (1) Sipe, J. E.; Boyd, R. W. *Phys. Rev. A* **1992**, *46*, 1614.
- (2) Kohlgraf-Owens, D. C.; Kik, P. G. *Opt. Express* **2009**, *17*, 15032.
- (3) Dittlbacher, H.; Felidj, N.; Krenn, J. R.; Lamprecht, B.; Leitner, A.; Aussenneq, F. R. *Appl. Phys. B: Laser Opt.* **2001**, *73*, 373.

- (4) Bakker, R. M.; Yuan, H. K.; Liu, Z.; Drachev, V. P.; Kildishev, A. V.; Shalaev, V. M.; Pedersen, R. H.; Gresillon, S.; Boltasseva, A. *Appl. Phys. Lett.* **2008**, *92*, 043101.
- (5) Moskovits, M. *Rev. Mod. Phys.* **1985**, *57*, 783.
- (6) Campion, A.; Kambhampati, P. *Chem. Soc. Rev.* **1998**, *27*, 241.
- (7) Bohren, C.; Huffman, D. *Absorption and Scattering of Light by Small Particles*; Wiley: New York, 1983.
- (8) Ruppin, R. *Surf. Sci.* **1983**, *127*, 108.
- (9) Takemori, T.; Inoue, M.; Ohtaka, K. *J. Phys. Soc. Jpn.* **1987**, *56*, 1587.
- (10) Ruppin, R. *Phys. Rev. B* **1992**, *45*, 11209.
- (11) Gozhenko, V. V.; Grechko, L. G.; Whites, K. W. *Phys. Rev. B* **2003**, *68*, 125422.
- (12) Nordlander, P.; Prodan, E. *Nano Lett.* **2004**, *4*, 2209.
- (13) García de Abajo, F. J. *Rev. Mod. Phys.* **2007**, *79*, 1267, and references therein.
- (14) Nordlander, P.; Le, F. *Appl. Phys. B: Laser Opt.* **2006**, *84*, 35.
- (15) Stuart, H. R.; Hall, D. G. *Phys. Rev. Lett.* **1998**, *80*, 5663.
- (16) Lal, S.; Westcott, S. L.; Taylor, R. N.; Jackson, J. B.; Nordlander, P.; Halas, N. J. *J. Phys. Chem. B* **2002**, *106*, 5609.
- (17) Maier, S. A.; Brongersma, M. L.; Kik, P. G.; Atwater, H. A. *Phys. Rev. B* **2002**, *65*, 193408.
- (18) Le, F.; Lwin, N. Z.; Steele, J. M.; Kall, M.; Halas, N. J.; Nordlander, P. *Nano Lett.* **2005**, *5*, 2009.
- (19) Le, F.; Lwin, N. Z.; Halas, N. J.; Nordlander, P. *Phys. Rev. B* **2007**, *76*, 165410.
- (20) Pinchuk, A.; Hilger, A.; von Plessen, G.; Kreibig, U. *Nanotechnology* **2004**, *15*, 1890.
- (21) Hilger, A.; Tenfelde, M.; Kreibig, U. *Appl. Phys. B: Laser Opt.* **2001**, *73*, 361.
- (22) Hilger, A.; Cuppers, N.; Tenfelde, M.; Kreibig, U. *Eur. Phys. J. D* **2000**, *10*, 115.
- (23) Mock, J. J.; Hill, R. T.; Degiron, A.; Zauscher, S.; Chilkoti, A.; Smith, D. R. *Nano Lett.* **2008**, *8*, 2245.
- (24) Féridj, N.; Aubard, J.; Lévi, G.; Krenn, J. R.; Schider, G.; Leitner, A.; Aussenegg, F. R. *Phys. Rev. B* **2002**, *66*, 245407.
- (25) Lévêque, G.; Martin, O. J. F. *Opt. Lett.* **2006**, *31*, 2750.
- (26) Lévêque, G.; Martin, O. J. F. *Opt. Express* **2006**, *14*, 9971.
- (27) Knight, M. W.; Wu, Y.; Lassiter, J. B.; Nordlander, P.; Halas, N. J. *Nano Lett.* **2009**, *9*, 2188.
- (28) Sonnichsen, C.; Geier, S.; Hecker, N. E.; von Plessen, G.; Feldmann, J.; Ditzbacher, H.; Lamprecht, B.; Krenn, J. R.; Aussenegg, F. R.; Chan, V. Z. H.; Spatz, J. P.; Moller, M. *Appl. Phys. Lett.* **2000**, *77*, 2949.
- (29) Schultz, S.; Smith, D. R.; Mock, J. J.; Schultz, D. A. *Proc. Nat. Acad. Sci. U.S.A.* **2000**, *97*, 996.
- (30) Mock, J. J.; Barbic, M.; Smith, D. R.; Schultz, D. A.; Schultz, S. *J. Chem. Phys.* **2002**, *116*, 6755.
- (31) Curry, A.; Nusz, G.; Chilkoti, A.; Wax, A. *Opt. Express* **2005**, *13*, 2668.
- (32) Klar, T.; Perner, M.; Grosse, S.; von Plessen, G.; Spirkl, W.; Feldmann, J. *Phys. Rev. Lett.* **1998**, *80*, 4249.
- (33) Sönnichsen, G.; Franzl, T.; Wilk, T.; von Plessen, G.; Feldmann, J.; Wilson, O.; Mulvaney, P. *Phys. Rev. Lett.* **2002**, *88*, 077402.
- (34) Novo, C.; Funston, A. M.; Pastoriza-Santos, I.; Liz-Marzan, L. M.; Mulvaney, P. *J. Phys. Chem. C* **2008**, *112*, 3.

JP911416A